ACS Photonics

Article

pubs.acs.org/journal/apchd5

Unraveling the Janus Role of Mie Resonances and Leaky/Guided Modes in Semiconductor Nanowire Absorption for Enhanced Light Harvesting

Diego R. Abujetas, Ramón Paniagua-Domínguez, and José A. Sánchez-Gil*

Instituto de Estructura de la Materia, Consejo Superior de Investigaciones Científicas, Serrano 121, 28006 Madrid, Spain

ABSTRACT: Light absorption from finite semiconductor nanowires is investigated through a unified theoretical picture and numerical simulations. We first show theoretically from the electromagnetic mode dispersion relation and the Mie extinction cross sections for infinite nanowires that formally equivalent (Janus) formulas yield both leaky/guided modes and Mie resonances as, respectively, complex wave vector or complex frequency solutions that, in turn, overlap only at grazing angles with respect to the nanowire axis. For finite semiconductor nanowires, the angle of incidence becomes critical: absorption is dominated by Mie resonances at incident angles perpendicular (and oblique) to the nanowire axis; by contrast, guided mode excitation (if spectrally available) governs and enhances absorption at grazing incidence. Such theoretical prediction can be exploited to optimize nanowire designs for broad band and broad angle light harvesting applications.

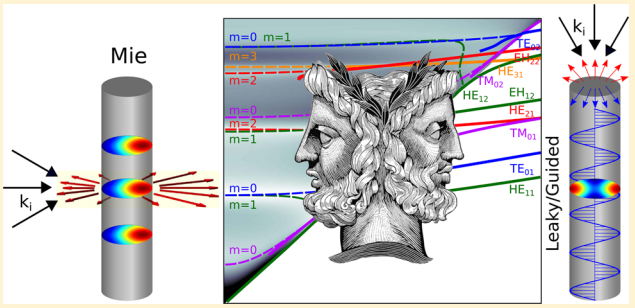

KEYWORDS: *semiconductor nanowire, Mie scattering, waveguide modes, light harvesting, photovoltaics*

Semiconductor nanowires (NWs) are attracting increasing interest in recent years. Among other fascinating applications, this stems from their unique optical properties,[1] which make them specially suitable to selectively enhance light scattering, absorption, and photoluminescence at the nanoscale.[1−7] The resulting realm of phenomenology, some in turn in connection with ad-hoc electronic and quantum properties, holds promise for potential single-photon sources and nanolasers,[8−11] solar light absorbers and photodetectors in photovoltaics,[2−4,12−17] antireflection coatings,[18] metamaterials,[19] and so on.

Particularly relevant to light harvesting applications are the enhanced absorption efficiencies of semiconductor NWs, specially when normalized by the volume of semiconductor material,[20] as revealed experimentally in recent years through a variety of configurations.[5,6,13,14,21−25] The phenomenon of light absorption at semiconducting NWs has been mostly described theoretically in two manners. On the one hand, it has been addressed in the context of light-coupling into leaky/guided modes,[5,20,23,25−28] well-known in electrodynamics for infinitely long NWs.[29−31] On the other hand, Mie light scattering from infinitely long cylinders[32] allows to interpret absorption and scattering properties of semiconducting NWs through Mie resonances.[33−37] Nonetheless, no clear connection between them has been formally established.

In this work, we first discuss theoretically the optical properties of infinitely long nanowires, indeed directly revealing the connection between Mie resonances and leaky modes in the corresponding equations, formally equivalent. Furthermore, we unify both theoretical pictures by subtly including Mie extinction cross sections at normal and oblique incidence onto the waveguide mode dispersion relation. This analysis allows to determine the appropriate nanowire dimensions and spectral regime for the ad-hoc coupling to (or excitation of) desired modes/resonances alike. On this basis, the unified theoretical picture is exploited also in connection with Mie absorption cross sections in order to shed light onto designing semiconducting nanowires for enhanced light absorption, showing numerical results for specific, finite-length nanowire configurations that allow also for guided mode excitation at grazing incidence.

RESULTS AND DISCUSSION

Infinite Cylinders: Leaky/Guided Modes versus Mie Resonances. First of all, we study the optical properties of infinitely long semiconducting nanowires through a scheme that accounts jointly for leaky/guided modes and Mie resonances. Leaky/guided modes in cylinders of radius R are obtained by solving the dispersion relation:[29]

$$\left[\frac{\mu_c}{u}\frac{J'_m(u)}{J_m(u)} - \frac{\mu}{v}\frac{H'_m(v)}{H_m(v)}\right]\left[\frac{\epsilon_c}{u}\frac{J'_m(u)}{J_m(u)} - \frac{\epsilon}{v}\frac{H'_m(v)}{H_m(v)}\right] = m^2\frac{(k_zR)^2}{(\omega R/c)^2}\left(\frac{1}{v^2} - \frac{1}{u^2}\right)^2 \quad (1)$$

Received: March 11, 2015
Published: June 3, 2015

DOI: 10.1021/acsphotonics.5b00112
ACS Photonics 2015, 2, 921−929

where $u = k_c R$, $v = kR$, m is an integer, and J_m and H_m are standard Bessel and (first-kind) Hankel functions; the transverse components of the mode wavevector at frequency ω, inside (k_c) and outside (k) the cylinder, are

$$k_c^2 = \epsilon_c \frac{\omega^2}{c^2} - k_z^2 \tag{2a}$$

$$k^2 = \epsilon \frac{\omega^2}{c^2} - k_z^2 \tag{2b}$$

k_z being the mode complex wavevector along the cylinder axis (see top panel in Figure 1) and $\omega/c = 2\pi/\lambda$ (λ is the wavelength in vacuum. The dielectric permittivities and magnetic permeabilities of the cylinder and embedding medium are ϵ_c, μ_c and ϵ, μ, respectively, with corresponding refractive indices $n = (\epsilon\mu)^{1/2}$ and $n_c = (\epsilon_c\mu_c)^{1/2}$. Throughout the rest of the paper, we assume the embedding medium to be vacuum $n = 1$ and nonmagnetic cylinders ($\mu_c = \mu = 1$). Thus, modes with $k_z < \omega/c$ ($k_z > \omega/c$) are leaky (guided). More specifically, $k_z = k_z' + ik_z''$ is real for guided modes ($k_z'' = 0$), so that k is purely imaginary for a lossless dielectric cylinder (the mode is confined inside the cylinder); by contrast, both k_z,k are complex for leaky modes, with $k_z'' > 0$ ($k'' < 0$) accounting for radiative losses along the propagation direction.[38]

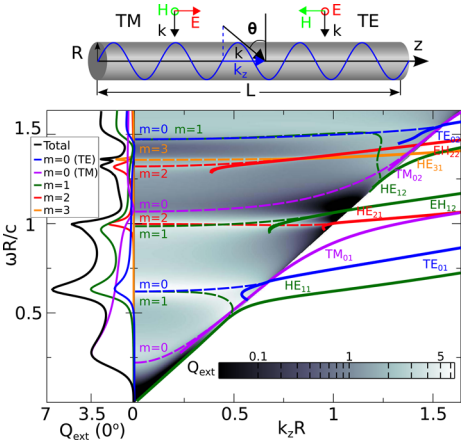

Figure 1. Top panel: Schematic of the Mie scattering configuration, including also the convention for the leaky/guided mode wavevectors used for their dispersion relations. Lower (center) graph: Dispersion relation $\omega R/c$ vs k_zR from eq 1 (solid curves) of the first leaky/guided modes of InP nanowires with varying radius R at $\lambda = 532$ nm (refractive index $n_c = n_{InP} = 3.7$). The spectral dependence of the extinction efficiency $Q_{ext} \equiv Q_{sca}$ is superimposed as a contour map within the light cone, calculated through Mie scattering (TE and TM polarization, eqs 4) for varying angle of incidence θ such that $k_z = (\omega/c)\sin\theta$ ($\theta = 90°$ coincides with the light line). The complex (Mie-like, see text) $\omega(k_z)$ solutions of eq 5 for real $ck_z/\omega = ck_z'/\omega$ are also included (dashed curves). Left graph: Q_{ext} at $\theta = 0°$, including the lowest-order (up to $m = 3$) contributions (for $m = 0$, TE and TM polarizations are shown separately).

Let us focus on an InP nanowire in vacuum at a wavelength in the visible, that is, $\lambda = 532$ nm. As a first approach, for the sake of simplicity that will allow a better understanding, the InP refractive index[39] is assumed to be real: $n_c = n_{InP} = 3.7$ (absorption is neglected). The dispersion relation is calculated from eq 1 in terms of $\omega R/c$ versus $k_z'R$ (recall that $k_z = k_z' + ik_z''$ is complex). This means that, strictly speaking, the nanowire radius R is the independent variable, whereas $\omega = 2\pi/\lambda$ remains fixed; alternatively, as long as the refractive index remains constant, the resulting dispersion relation can also be applied to a proper spectral dependence for fixed nanowire radius R. In this manner, we do not incorporate in the discussion the spectral dependence of the semiconductor refractive index (nor that of the absorption), which will be dealt with in connection with light absorption spectra later on.

The results are shown in Figure 1: the light line $\omega/c = k_z$ separates the guided modes $k_z' \geq \omega/c$ from the leaky modes $k_z' < \omega/c$. The latter modes thus leak out of the NW due to the nonnegligible wavevector component in the plane perpendicular to the NW axis, unlike guided modes. Leaky modes are continued outside the light cone into guided modes as long as their symmetry is preserved (same notation in Figure 1) and will be discussed below. In the case of $m = 0$ in eq 1, transverse electric (TE_{0m}) and magnetic (TM_{0m}) modes are decoupled, satisfying each set the following dispersion relations:

$$\frac{\epsilon_c}{u}\frac{J'_m(u)}{J_m(u)} - \frac{1}{v}\frac{H'_m(v)}{H_m(v)} = 0, \quad \text{for TE modes} \tag{3a}$$

$$\frac{1}{u}\frac{J'_m(u)}{J_m(u)} - \frac{1}{v}\frac{H'_m(v)}{H_m(v)} = 0, \quad \text{for TE modes} \tag{3b}$$

The lowest ($m = 1$) electromagnetic (EM) mode is referred to as HE_{11}, exhibiting no cutoff in the low energy limit $\omega = 0$. Conversely, for fixed ω, this no-cutoff mode HE_{11} is present also no matter how thin the NW might be. Nonetheless, in such $\omega R \to 0$ limit, this hybrid mode becomes very weakly guided, its electromagnetic field being mainly localized into the surrounding medium,[7] with no significant impact on absorption.

On the other hand, Mie resonances are determined by calculating the extinction Q_{ext}, scattering Q_{sca}, and absorption Q_{abs} efficiencies from the following expressions for TE and TM polarization:[32]

$$Q_{ext}^{(TE)} = \frac{2}{kR}\Re\left[a_{0II} + 2\sum_{m=1}^{\infty} a_{mII}\right] \tag{4a}$$

$$Q_{ext}^{(TM)} = \frac{2}{kR}\Re\left[b_{0I} + 2\sum_{m=1}^{\infty} b_{mI}\right] \tag{4b}$$

$$Q_{sca}^{(TE)} = \frac{2}{kR}\left[|a_{0II}|^2 + 2\sum_{m=1}^{\infty}(|a_{mII}|^2 + |b_{mII}|^2)\right] \tag{4c}$$

$$Q_{sca}^{(TM)} = \frac{2}{kR}\left[|b_{0I}|^2 + 2\sum_{m=1}^{\infty}(|b_{mI}|^2 + |a_{mI}|^2)\right] \tag{4d}$$

$$Q_{abs} = Q_{ext} - Q_{sca} \tag{4e}$$

where a_{mI}, b_{mI}, a_{mII}, and b_{mII} are the corresponding Mie scattering coefficients[32] for a plane wave impinging on the infinite nanowire (see top panel in Figure 1), polarized either parallel (TM) or perpendicular (TE) to the plane defined by the NW axis and the incident wavevector at the oblique angle of incidence θ.

First of all, let us discuss whether a connection can be established between a Mie resonance and a leaky/guided mode. This connection has been pointed out in refs 5 and 37, being unequivocally shown for a particular (TM_{01}) leaky mode and

DOI: 10.1021/acsphotonics.5b00112
ACS Photonics 2015, 2, 921−929

(lowest-order, TM polarized) Mie resonance.[37] However, a proper formal expression has not been derived yet. Mie resonances are obtained from the zeros of the denominators of the Mie scattering coefficients a_{nI}, b_{nI}, a_{nII}, and b_{nII}. It turns out that all coefficients share the same denominator,[32] so that the Mie resonance condition can be written as

$$\begin{aligned} & i\xi^2[\xi J'_m(\eta)H_m(\xi) - \eta J_m(\eta)H'_m(\xi)] \\ & \quad \times [n_c^2 \xi J'_m(\eta)H_m(\xi) - \eta J_m(\eta)H'_m(\xi)] \\ & \quad - i\left[m\eta \sin\theta J_m(\eta)H_m(\xi)\left(\frac{\xi^2}{\eta^2} - 1\right)\right]^2 = 0 \end{aligned} \tag{5}$$

where $\xi = (\omega R/c)\cos\theta$ and $\eta = (\omega R/c)(\epsilon_c - \sin^2\theta)^{1/2}$. If we identify the incident wavevector component along the cylinder axis as $k_z = (\omega/c)\sin\theta$, it follows that $\xi = v$ and $\eta = u$. Then, after some algebraic manipulation, the latter equation can be rewritten as

$$\begin{aligned} & -i[uv^2 J_m(u)H_m(v)]^2 \\ & \times \left\{\left[\frac{\mu_c}{u}\frac{J'_m(u)}{J_m(u)} - \frac{\mu}{v}\frac{H'_m(v)}{H_m(v)}\right]\right. \\ & \times \left[\frac{\epsilon_c}{u}\frac{J'_m(u)}{J_m(u)} - \frac{\epsilon}{v}\frac{H'_m(v)}{H_m(v)}\right] \\ & \left. - m^2\frac{(k_z R)^2}{(\omega R/c)^2}\left(\frac{1}{v^2} - \frac{1}{u^2}\right)^2\right\} = 0 \end{aligned} \tag{6}$$

upon imposing that the term in braces is equal to zero, we retrieve a condition formally identical to eq 1 above.

To illustrate our procedure, we focus again on an InP nanowire in vacuum ($n = 1$) at $\lambda = 532$ nm, as in Figure 1, including the analysis of Mie resonances in the same graph in the following manner. The unpolarized extinction (or scattering, since absorption is neglected thus far) efficiency, $Q_{ext} = (Q_{ext}^{(TE)} + Q_{ext}^{(TM)})/2$, for the same nanowire parameters, is plotted for an incident plane wave (TE and TM polarization) as a color map, by assuming that k_z is connected to the wavevector component along the nanowire axis $k_z = (\omega/c)\sin\theta$ (see Figure 1, inset). To make it more evident, we have solved eq 1 for complex $\omega(k_z)$ solutions for real $ck_z/\omega = \sin\theta$ in the nonradiative region; these Mie resonances are superimposed in Figure 1 (dashed curves), lying alongside the maxima of the Mie extinction efficiencies throughout the light cone and connecting with corresponding leaky modes for large k_z, thus, confirming a formal equivalence that resembles the two faces of "Janus bifrons". The resulting scheme enables us to understand the complex interplay between leaky modes and Mie resonances in a relatively simple manner. [Incidentally, it should be noted that the Mie resonances are red-shifted with regard to the extinction maxima in Figure 1; this is connected with the asymmetric (Fano-like) line shape of Mie resonances in cylinders.[40]]

Nonetheless, note that the correspondence between them is subtle. This stems from the fact that leaky modes are complex $k_z(\omega)$ zeros, at real ω, of the above eq 3, whereas Mie resonances arise as complex $\omega(k_z)$ zeros, at real $ck_z/\omega = \sin\theta$. The imaginary part of the leaky mode yields the mode decay rate due to leakage (and absorption if present) along propagation. By contrast, the imaginary part of the Mie resonance frequency yields the resonance width due to scattering (and absorption if present). Therefore, such correspondence manifests as a direct overlap in the k_z–ω plane only when the leaky modes possess very small k''_z (large decay lengths, or low radiation losses) and the Mie resonance has a small width ω''. This predominantly occurs when the leaky mode dispersion curve yields large k'_z, actually close to the light line at ω/c, in turn, overlapping with Mie resonances at large, oblique angle of incidence θ. For small angles of incidence θ, $k_z = (\omega/c)\sin\theta \to 0$, the existing leaky modes exhibit large k''_z (not shown in Figure 1), and no direct overlap with its corresponding Mie resonance is observed in the k_z–ω plane. In general, leaky modes should play a leading role in point dipole excitations,[41] whereas Mie resonances properly account for plane wave scattering[37] (at least over a wide angular range), as is the case of NW absorption studied herein.

To shed more light on this argument, let us plot the EM field patterns associated with the lower $m = 0$, 1 leaky/guided modes, which in turn determine their symmetry, as shown in Figure 2. First, we focus on the leaky modes exhibiting the

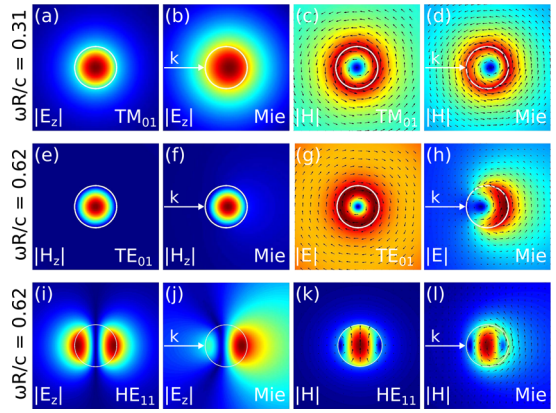

Figure 2. (a, c, e, g, i, k) Contour maps of the intensity of the relevant EM field components of the two lowest-order leaky modes and the first guided mode of an infinite InP cylinder at $\lambda = 532$ nm (refractive index $n_{InP} = 3.7$): (a, c) TM_{01} mode for radius $R = 26.25$ nm, which corresponds to $\omega R/c = 0.31$ in Figure 1. (e, g) TE_{01} mode for radius $R = 52.5$ nm, which corresponds to $\omega R/c = 0.62$ in Figure 1. (i, k) HE_{11} guided mode for radius $R = 52.5$ nm, which corresponds to $\omega R/c = 0.62$ in Figure 1. (b, d, f, h, j, l) Correspondingly, contour maps of the intensity of the total EM field components resulting from the plane wave scattering by the same InP cylinders (the white arrow indicates the in-plane incident wavevector, with $\theta = 0°$, out-of-plane component $k_z = 0$), for the frequencies/radii exciting the three lowest order Mie resonances: (b, d) TM-polarized ($m = 0$) Mie resonance for radius $R = 26.25$ nm, which corresponds to $\omega R/c = 0.31$ in Figure 1. (f, h) TE-polarized ($m = 0$) Mie resonance for radius R = 52.5 nm, which corresponds to $\omega R/c = 0.62$ in Figure 1. (j, l) HE ($m = 1$) Mie resonance (excited with TM-polarized light) for radius $R = 52.5$ nm, which corresponds to $\omega R/c = 0.62$ in Figure 1. The small black arrows in (c, d, g, h, k, l) indicate directions of the in-plane electric or magnetic field vectors.

lowest-order TM_{01} and TE_{01} symmetries (see Figure 2a,c,e,g); the EM field pattern associated with the $m = 0$ Mie resonance obtained by illuminating the same nanowires with either TM or TE polarized plane wave at $\theta = 0°$ are shown in Figure 2b,d,f,h, respectively, revealing a strong resemblance with their associated leaky modes, as expected. With regard to the lowest $m = 1$ Mie resonance, note that no associated leaky mode exists; in fact, it redshifts for large angles and approaches the light line along with the no cutoff HE_{11} guided mode, which

DOI: 10.1021/acsphotonics.5b00112
ACS Photonics 2015, 2, 921–929

remains (weakly) guided in the low energy limit (overlapping with the light line). Thus, we show instead the EM field pattern of the HE_{11} guided mode in Figure 2i,k, which strongly resembles the symmetry of such lowest $m = 1$ Mie resonance (Figure 2j,l), revealing their connection. Note that, despite the unambiguous resemblance in all cases, the plane wave illumination associated with the Mie scattering results introduces certain asymmetry with respect to their corresponding (highly symmetric) leaky/guided mode patterns.

Moreover, from the dispersion relation shown in Figure 1, guided modes in the nonradiative region are related to leaky modes across the light line,[41] and in turn to their corresponding Mie resonances, even if strongly shifted in $\omega R/c$. This is supported by the EM field patterns, which manifest their analogue symmetries, as shown above.

Finite NWs: Mie Resonances and Leaky Modes. In order to address light absorption by finite NWs, Mie resonances (and, correspondingly, leaky modes) of the infinite NW ought to be studied first. This can be done as in Figure 1, but properly taking into account the dispersive behavior of the semiconductor in the spectral regime of interest, including of course absorption. This is shown in Figure 3 for an InP cylinder of radius $R = 20$ nm for vacuum wavelengths covering the visible and NIR domains up to $\lambda = 0.8$ μm. Within this spectral regime, such InP cylinder supports only the lowest-order leaky mode TM_{01}, and the very weakly guided (no cutoff) HE_{11} mode: the radius of the NW ($R = 20$ nm) is chosen so that coupling into the TM_{01} leaky mode predominates in the visible (high absorption). The corresponding $m = 0$ Mie resonance is clearly observed as a bright band in the extinction/absorption efficiencies, in turn, associated with such leaky mode.

To distinguish the impact of spectral dispersion from that of absorption, we have plotted in Figure 3a the leaky mode dispersion relation and Mie extinction efficiency (with corresponding resonance) neglecting absorptive losses Im-$(n_{InP}(\omega)) = 0$. Dispersion of $\mathrm{Re}(n_{InP}(\omega))$ indeed induces a bending of the lowest-order ($m = 0$) Mie resonance $E \gtrsim 3$ eV; recall that this Mie resonance exhibits the symmetry of the TM_{01} mode. Upon introducing absorption (see Figure 3b), the Mie resonance is substantially broadened, mainly at frequencies beyond $E \geq 2.5$ eV ($\lambda \leq 500$ nm) where InP exhibits large absorption coefficients. Consequently, larger absorption efficiencies are thus expected in such spectral domain, in turn coinciding for this NW radius with Mie resonances and leaky modes. To distinguish the polarization dependence of the absorption bands, we plot in Figure 3c,d each contribution separately. As expected, the TM-polarized Mie resonance at near-normal incidence is only excited with TM-polarized incident light.

Moreover, the (polar) angular span of the absorption bands can also be predicted from Figure 3b, as inferred from the $k_z = (\omega/c)\sin\theta$ dependence of the absorption efficiencies (shown in Figure 3c,d). In fact, broad angle absorption is observed in Figure 3d for the $m = 0$ Mie resonance with a broad maximum at $\theta \sim 50°$, associated with the overlap with the TM_{01} leaky mode excitation; recalling that the extinction maximum without absorption (Figure 3a) occurs at $\theta = 0°$ coinciding with the $m = 0$ TM mode, this indicates that absorption is somewhat enhanced at large angles through leaky mode coupling.

We now investigate the spectral/angular dependence of the absorption efficiency for finite NWs through COMSOL numerical calculations, exploiting the physical insight provided above with regard to Mie resonances and leaky modes. We

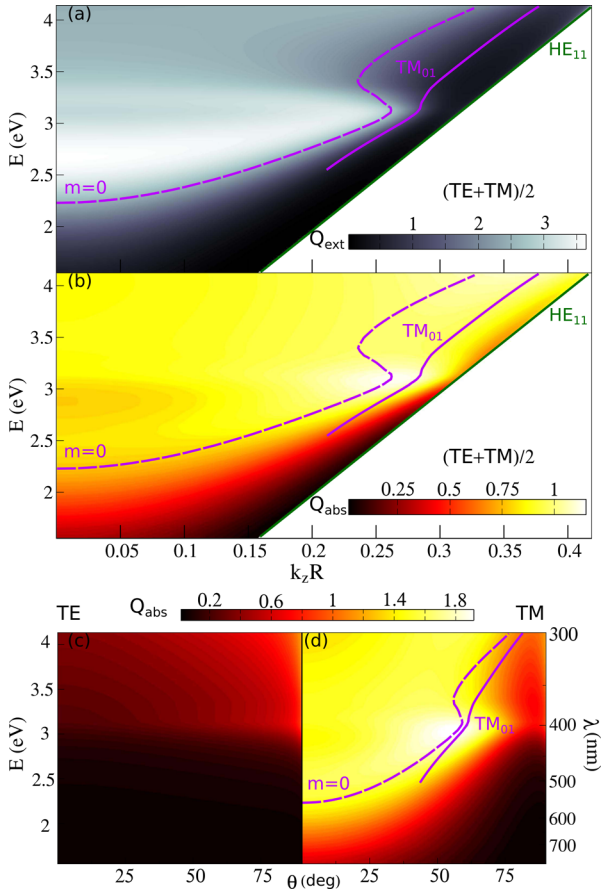

Figure 3. (a, b) The spectral dependence of the corresponding unpolarized Mie efficiency Q within the light cone as a contour map, calculated through Mie scattering (TE and TM polarization) for varying angle of incidence θ such that $k_z = (\omega/c)\sin\theta$, for InP nanowires of radius $R = 20$ nm, fully taking into account the complex, frequency-dependent InP refractive index $n_{InP}(\omega)$. (a) Absorptive losses are neglected $\mathrm{Im}(n_{InP}(\omega)) = 0$ and the extinction efficiency Q_{ext} is plotted; (b) Absorptive losses are fully accounted for and the absorption efficiency Q_{abs} is shown instead. (c, d) Same as in (b), but for TE (c) and TM (d) polarization separately as a function of the angle of incidence θ. In all cases, the dispersion relation $E = \hbar\omega$ (eV) vs k_zR of leaky/guided modes from eq 1 is superimposed (solid curves), along with the complex (Mie-like, see text) $\omega(k_z)$ resonances (dashed curves), both for $\mathrm{Im}(n_{InP}(\omega)) = 0$.

show in Figure 4 the absorption efficiency Q_{abs} for a finite InP NW of radius $R = 20$ nm and length $L = 3$ μm, presented as in Figure 3b,c,d. It should be noted that numerical absorption cross sections have been normalized to match Mie absorption efficiencies as $Q_{abs} = C_{abs}/(2RL)$. In fact, Q_{abs} closely resembles that of an infinite NW obtained through Mie theory.

Next, we plot in Figure 5a,b the spectral dependence of the absorption efficiencies at $\theta = 0°,50°$ incidence, compared to that obtained for an infinite InP NW through Mie calculations. At normal incidence, the broad absorption band due to the lowest (TM, $m = 0$) Mie resonance is observed with two nearby local maxima ($\lambda = 400,500$ nm) due to the InP absorption dispersion, the numerical calculation for the finite NW being nearly identical to that of infinite-NW Mie absorption. Also, the absorption efficiency at $\theta = 50°$ incidence numerically calculated for a finite NW closely resembles the Mie efficiency for an infinite NW, exhibiting a maximum exactly at the position of the Mie resonance at $\lambda = 400$ nm. This

DOI: 10.1021/acsphotonics.5b00112
ACS Photonics 2015, 2, 921−929

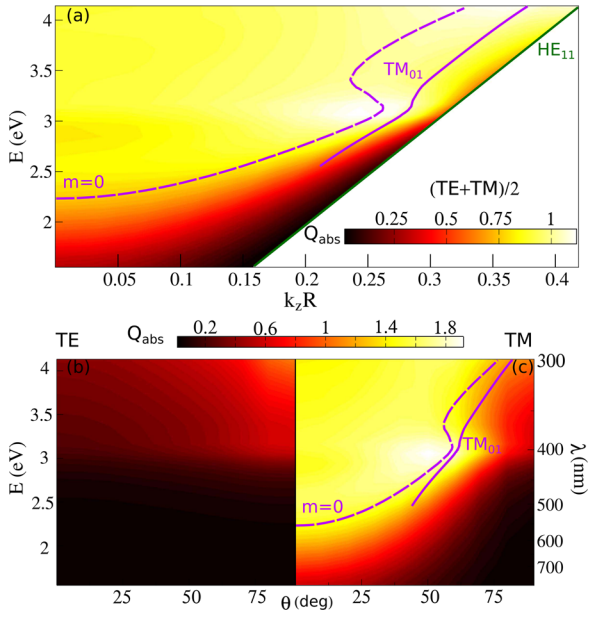

Figure 4. Contour map of the spectral dependence of the absorption cross section Q_{abs} for a finite InP nanowire of radius R = 20 nm and L = 3 μm, numerically calculated for varying angle of incidence θ such that $k_z = (\omega/c)\sin\theta$: (a) unpolarized and (b) TE and (c) TM polarization, separately. The dispersion relation $\omega R/c$ vs $k_z R$ of leaky/guided modes from eq 1 for an infinite InP nanowire of the same radius is superimposed (solid curves), along with the complex Mie $\omega(k_z)$ resonances (dashed curves), both for $\mathrm{Im}(n_{InP}(\omega)) = 0$.

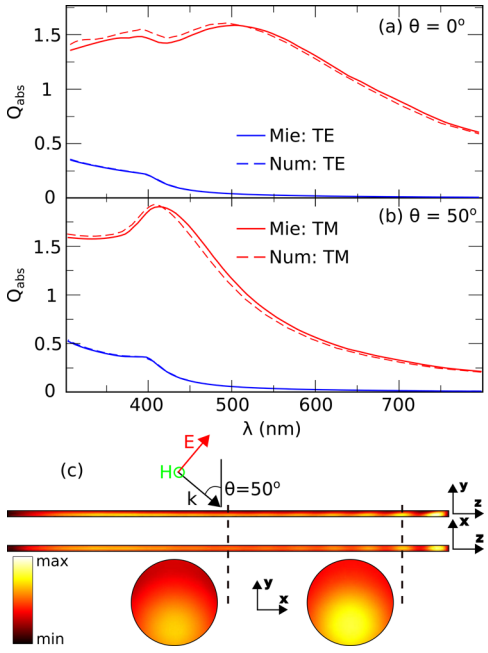

Figure 5. (a, b) Spectral dependence of the absorption efficiencies $Q_{abs}(\lambda)$ for an InP nanowire of radius R = 20 nm, obtained from Figure 3c,d (Mie calculation for an infinite NW, solid curves) and from Figure 4b,c (numerical calculations for a finite NW of length L = 3 μm, dashed curves), for the angles of incidence θ = 0°,50°. (c) Corresponding near-field images of the total absorbed power inside the NW at λ = 400 nm for θ = 50°, for two planes along the NW and for two transverse cross sections, as depicted.

correspondence is somewhat expected for a wide angular range perpendicular to the NW axis. At parallel incidence one could expect the impact of the NW finiteness to become stronger, since coupling to guided modes (forbidden in the infinite case) is allowed. However, only the HE_{11} (no cutoff) guided-mode is present for such a thin NW and turns out to be very weakly guided in this spectral regime: most of the EM energy in the mode is localized outside the NW (i.e., the mode area is very large) so that absorption is not efficiently enhanced. Therefore, for thin (and sufficiently long) NWs in the absence of other (higher-order) guided modes, absorption is fully described by Mie theory for infinitely long NWs, its maximum stemming from the lowest (TM, m = 0) Mie resonance (nearly indistinguishable from the contribution from its leaky-mode counterpart). For thicker NWs supporting strongly coupled guided modes, the general principle holds, as expected, and the absorption efficiency for the finite NW might differs from the Mie Q_{abs}, as will be described below.

Let us further explore the physical mechanisms underlying the strong absorption enhancements observed. Recall that, close to parallel incidence, Mie resonances nearly coincide with their leaky modes of analogous symmetry close to the light line, due to the fact that their widths (in the ω and k_z space, respectively) are very small, as mentioned above. Light impinging obliquely onto the NW couples into leaky modes and is absorbed more efficiently than at normal incidence (regardless of the NW finiteness). To illustrate this effect, contour maps of the absorbed power $\langle P_{abs}\rangle = (\pi c/\lambda)\mathrm{Im}(\varepsilon_c)|E|^2$ are shown in Figure 5c for the absorption maximum: large absorption is observed throughout the NW, which no doubt results from the m = 0 TM Mie resonance, correlated with the TM_{01} leaky mode excitation, as confirmed by the transverse patterns (see Figure 2a,b). However, unlike for an infinite NW, the absorbed power is not uniform along the NW, but exhibits some oscillations, especially near the NW end opposite to the incident light, resulting from diffraction effects. Upon averaging along the NW, though, the absorbed power is nearly identical to that of a segment of length L of an infinite NW, so that $C_{abs} = 2RLQ_{abs}^{Mie}$.

Finite NWs: Role of Guided Modes. In the previous section, the InP NW radius was such that no absorption stemming from guided modes might take place in the visible (spectral region with higher absorption for InP). Since coupling to guided modes, though forbidden for infinitely long cylinders, is plausible at finite NWs due to the light scattering at the NW end-facets,[37] we now consider a thicker InP NW that supports at least a guided mode in the visible. Again, we investigate first the Mie resonances (and, correspondingly, leaky modes) of the infinite NW, properly taking into account the dispersive behavior of the semiconductor in the spectral regime of interest as in Figure 3. This is shown in Figure 6 for an InP cylinder of radius R = 40 nm for vacuum wavelengths covering the visible and NIR domains: Within this spectral regime, such InP NWs support various lowest-order leaky/guided modes TE_{01}, TM_{01}, and HE_{11}.

Bright bands in the extinction/absorption efficiencies are clearly observed at normal incidence that extend over most of the angular range due to the Mie resonances and associated leaky modes. As in Figure 3a, we have plotted in Figure 6a the dispersion relations of Mie resonances (dashed curves) and leaky/guided modes (solid curves), along with the Mie extinction efficiency, neglecting in all cases absorptive losses $\mathrm{Im}(n_{InP}(\omega)) = 0$: Note that InP dispersion now induces significant splittings in various modes. Among them, the m = 0 TE Mie resonance is remarkably split into three flat branches,

DOI: 10.1021/acsphotonics.5b00112
ACS Photonics 2015, 2, 921−929

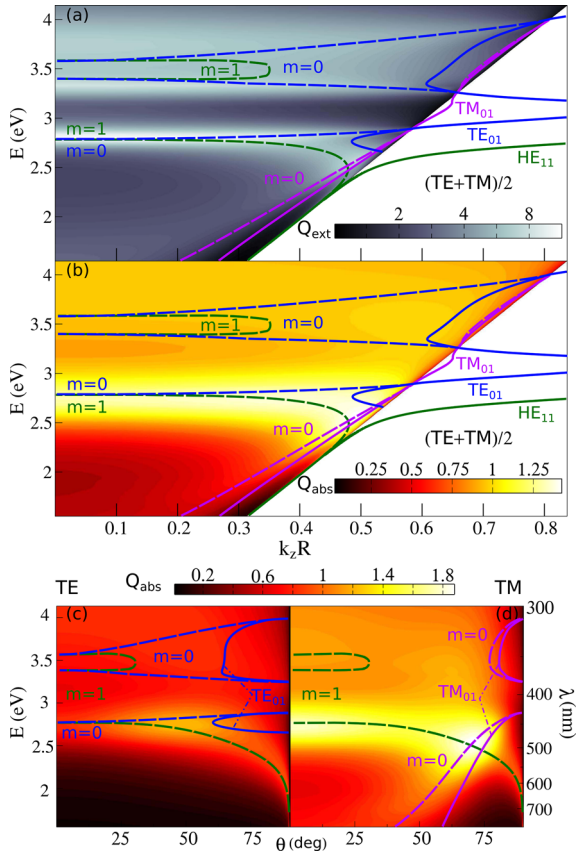

Figure 6. (a, b) The spectral dependence of the corresponding unpolarized Mie efficiency Q within the light cone as a contour map, calculated through Mie scattering (TE and TM polarization) for varying angle of incidence θ such that $k_z = (\omega/c)\sin\theta$, for InP nanowires of radius R = 40 nm, fully taking into account the complex, frequency-dependent InP refractive index $n_{InP}(\omega)$. (a) Absorptive losses are neglected $\mathrm{Im}(n_{InP}(\omega)) = 0$ and the extinction efficiency Q_{ext} is plotted; (b) Absorptive losses are fully accounted for and the absorption efficiency Q_{abs} is shown instead. (c, d) Same as in (b), but for TE (c) and TM (d) polarization separately as a function of the angle of incidence θ. In all cases, the dispersion relation $E = \hbar\omega$ (eV) vs k_zR of leaky/guided modes from eq 1 is superimposed (solid curves), along with the complex Mie $\omega(k_z)$ resonances (dashed curves), both for $\mathrm{Im}(n_{InP}(\omega)) = 0$.

all of them with the symmetry of the TE_{01} mode (not shown here). The m = 1 Mie resonance (with a hybrid TM and TE character analogous to the HE_{11} mode) exhibits two branches, the upper-one indeed bending over itself. The impact of dispersion on the lowest-order m = 0 TM Mie resonance is smaller: its lower branch, lying below 2.7 eV, barely changes; nonetheless, an upper branch emerges very close to the light line in the region 3.2−4 eV. At large angles, the corresponding TE_{01} and TM_{01} leaky modes appear, also exhibiting complicated band structures: the two curved branches of the leaky TE_{01} leading to three corresponding guided bands outside the light cone (strictly speaking, there are only two, since the lower two bands are bent/connected at higher k_z), and the alternating leaky/guided character of the TM_{01} mode, with a small guided band within 2.7−3.2 eV. As expected for the sake of symmetry, the TE_{01} and TM_{01} modes cross the light line in all cases at the same frequency. On the other hand, note that the lowest guided HE_{11} mode remains largely unaltered and connects with the lowest m = 1 Mie band along the light line toward the low energy limit. However, the guided band also bends in the highly dispersive region around 3 eV, not shown since it lies beyond the k_zR scale covered in Figure 6a.

Upon introducing absorption (see Figure 6b), Mie resonances are substantially broadened and even smeared out, as expected; for the sake of clarity, Figure 6c,d shows the absorption efficiencies and mode dispersion for TE and TM polarization separately as a function of the angle of incidence θ. In fact, broad band and broad angle absorption is expected for the lowest m = 1 Mie resonances (HE_{11} mode) shown therein, indeed occurring for both TM- and TE-polarized light (see Figure 6c,d), being stronger at normal incidence for TM polarization.[28] In addition, Figure 6d reveals that the TM_{01} leaky mode band lies, as mentioned in the preceding section, close to the m = 0 TM Mie resonance at large oblique angles, which yields a large absorption area at ∼2.5 eV (500 nm) near $\theta \simeq 70°$, as a result in turn of the overlap with the m = 1 Mie band. In the low energy region below 2.5 eV, this m = 0 TM Mie resonance continues, as mentioned above, as a weak absorption band for smaller angles of incidence. The lowest m = 0 TE Mie branch yields a weaker absorption maximum in Figure 6c for $\theta \simeq 50°$ at ∼450 nm. In the blue part of the spectrum and into the UV, InP absorptive losses increase, so that the above-mentioned upper branches of the m = 0 TE and m = 1 hybrid Mie resonances result in (spectrally and angularly) broadened bands of moderate absorption.

We now calculate numerically the absorption cross section in the case of a finite NW, as shown in Figure 7 for L = 3 μm. $Q_{abs}(\omega,\theta)$ closely resembles from a qualitative standpoint that of an infinite NW obtained through Mie theory (see Figure 6b−d) at normal incidence, confirming (i) the m = 0,1 Mie resonances at $\lambda \sim$ 450 nm; (ii) a broad absorption region in the

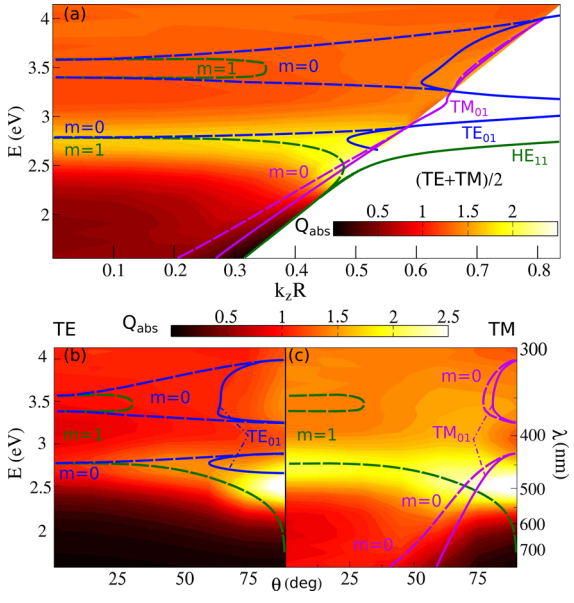

Figure 7. Contour map of the spectral dependence of the absorption cross section Q_{abs} (both TE and TM polarization) for a finite InP nanowire of radius R = 40 nm and L = 3 μm, numerically calculated for varying angle of incidence θ such that $k_z = (\omega/c)\sin\theta$: (a) Unpolarized and (b) TE and (c) TM polarization, separately. The dispersion relation $\omega R/c$ vs k_zR of leaky/guided modes from eq 1 for an infinite InP nanowire of the same radius is superimposed (solid curves), along with the Mie $\omega(k_z)$ resonances (dashed curves), both for $\mathrm{Im}(n_{InP}(\omega)) = 0$.

DOI: 10.1021/acsphotonics.5b00112
ACS Photonics 2015, 2, 921−929

UV part of the spectra ($E > 3$ eV, $\lambda < 400$ nm), where the (split) branches of the $m = 0$ (TE) and $m = 1$ (hybrid HE_{11}) Mie resonances are smeared out due to the strong InP absorption. Nevertheless, a significantly brighter (more absorptive) area near 2.5 eV ($\lambda = 500$ nm) appears at grazing $\theta = 90°$ incidence in Figure 7a, which differs from all the other bands lying nearby for an infinite NW ($m = 0,1$ Mie resonances and the two $m = 0$, TE and TM leaky bands, see Figure 6b–d): it is clearly a polarization-independent, grazing-angle excitation (see Figure 7b,c) occurring only for a finite NW. In addition to this bright band, higher absorption is observed in the finite NW at grazing incidence into the UV region, presumably owing to the interplay with the complex upper branches of the $m = 0$ (TE and TM) leaky/guided modes.

To make clear the differences, we also plot in Figures 8 and 9 the spectral dependence of the absorption efficiencies Q_{abs} at

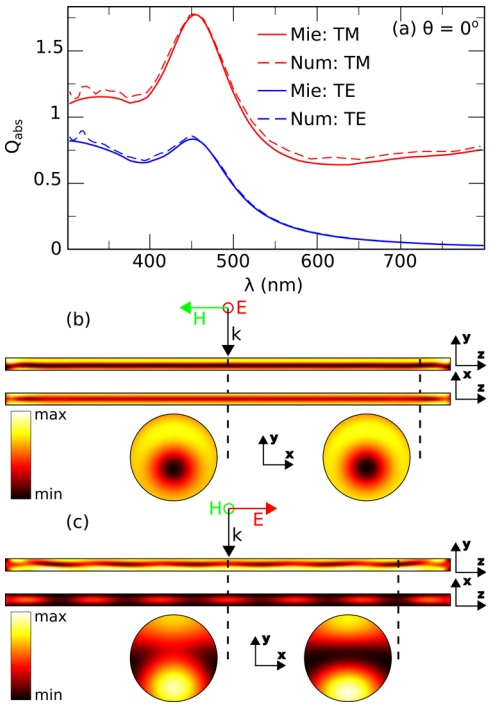

Figure 8. (a) Spectral dependence of the absorption efficiencies $Q_{abs}(\lambda)$ for an InP nanowire of radius $R = 40$ nm, obtained from Figure 6c,d (Mie calculation for an infinite NW) and Figure 7b,c (numerical calculations for a finite NW of length $L = 3$ μm), for the angle of incidence $\theta = 0°$. (b,c) Corresponding near-field images of the total absorbed power inside the NW at $\lambda = 450$ nm for (b) TE and (c) TM polarization for two planes along the NW, including also two transverse cross sections, as depicted.

parallel and perpendicular incidence, compared to that obtained for an infinite InP NW through Mie calculations. At incidence perpendicular to the NW axis (see Figure 8a), the absorption efficiency numerically calculated for a finite NW closely resembles the Mie efficiency for an infinite NW, exhibiting maxima exactly at the frequency of both Mie resonances (which coincide). Incidentally, the contour maps showing the absorbed power in Figure 8b,c nicely manifest the interplay of those two modes: TE polarization seems to predominantly couple to the $m = 0$ (TE) Mie resonance (compare Figure 8c to the mode patterns in Figure 2g,h); whereas TM polarization (Figure 8c) can only couple into the $m = 1$ (HE_{11}) hybrid resonance (see Figure 2i,j). It should be recalled that this hybrid mode

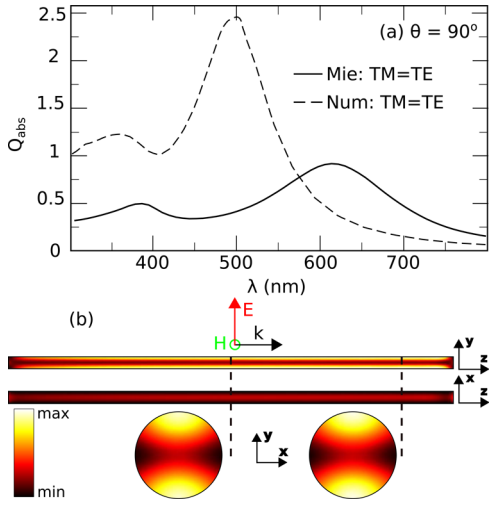

Figure 9. (a) Same as in Figure 8 but for $\theta = 90°$. (b) Corresponding near-field images of the total absorbed power inside the NW at $\lambda = 500$ nm for $\theta = 90°$, for two planes along the NW, including also two transverse cross sections, as depicted.

becomes predominantly TM near normal incidence, as pointed out also in ref 28, thus being weakly excited by TE light (as mentioned above). In any case, Mie calculations for an infinite NW reproduce very accurately the absorption efficiencies for finite NWs (see Figure 8a), and fairly well the EM fields inside the NW, except for some weak oscillations associated with finite size diffraction (as commented in the preceding section). These similarities extend over a wide angular range up to grazing incidence.

At parallel incidence, however, the impact of the NW finiteness becomes stronger and the absorption efficiency for the finite NW differs both qualitatively and quantitatively from the Mie Q_{abs} (see Figure 9a). The absorption maximum is slightly blue-shifted, and more importantly, remarkably larger for the finite NW throughout the UV. In fact, this larger, blue-shifted maximum does not correspond to the (TM, $m = 0$) Mie resonance; rather, it is due to the (NW-finiteness-induced) excitation of the lowest-order HE_{11} guided mode, as demonstrated below.

Recently, a very similar configuration has been experimentally described,[37] theoretically demonstrating that guided modes come into play at such NW radii, since light scattering at the finite NW end-facets provides the extra momentum (phase matching) to allow coupling. In this particular range, it is the HE_{11} guided mode the one responsible of such coupling and the associated enhanced absorption. Recall that, unlike for the $R = 20$ nm NW, the HE_{11} guided mode becomes for this thicker NW radius ($R = 40$ nm) a properly guided mode with significant electric field intensity inside the NW at the spectral regime where absorption is relevant. Transverse and longitudinal contour maps of the power $\langle P_{abs} \rangle$ absorbed along the NW, shown in Figure 9b for the absorption maximum at grazing incidence, support this reasoning: large absorption is observed throughout the NW with the HE_{11} guided-mode symmetry (see also Figure 2i,j).

Therefore, although Mie scattering theory provides useful insight into the absorption efficiency of finite NWs associated with Mie resonance and leaky-mode excitation for a broad angular range, it largely underestimates absorption at incidence nearly parallel to the NW axis, leading to enhanced guided

DOI: 10.1021/acsphotonics.5b00112
ACS Photonics 2015, 2, 921–929

mode coupling (forbidden in infinite NWs), which in turn provides strong absorption cross sections. A contour map of $C_{abs} = 2RLQ_{abs}$ properly accounting for the finite NW length, such as those depicted in Figures 4 and 7, is needed to properly tune and enhance absorption, carefully accounting for the dispersive behavior of the semiconductor material in the spectral region of interest (large absorption).

For light incident near normal to the NW axis, Mie scattering faithfully predicts absorption. Thus, the NW dimensions can be correspondingly tuned to match a large, Mie-resonant absorption band (or bands), in turn continued as a leaky mode for very large angles of incidence, which can conveniently be split into two (or more) bands (for broad band absorption) due to the InP (and other semiconductor) refractive index dispersion. Near grazing incidence, guided modes should also be tuned to remarkably boost absorption for finite NWs due to light scattering at the NW end-facets. Furthermore, if broad angle incidence is experimentally feasible, our theoretical analysis reveals that both kinds of absorption mechanisms can coincide in a broad spectral region, thus leading to remarkably large absorption efficiencies. Thicker NWs can also be considered supporting several guided modes,[23] very likely enhancing absorption cross sections at the expense of diminishing efficiencies.

CONCLUSION

In this work, we have investigated theoretically and numerically light absorption in finite semiconducting NWs. First, we make use of the leaky mode dispersion relation and Mie scattering theory, showing in turn that a close relation exists between leaky/guided modes and Mie resonances, which stems from a formally equivalent equation, as the two faces of Janus bifrons. In light of this equivalence, means are given to graphically display such a relationship by subtly including Mie extinction/scattering/absorption cross sections at normal and oblique incidence, along with their corresponding Mie resonant frequencies, onto a leaky/guided mode dispersion relation. This unified picture is then exploited for the purpose of designing nanowires with ad-hoc optical properties, as shown in a variety of configurations. Conditions for broad-band, broad-angle, enhanced absorption efficiencies are investigated on the basis of the spectral and angular dependence of Mie resonance (likewise, leaky mode) excitation. Incidentally, we have found that, in the case of InP (and of many other similar semiconductors), the dispersion of the (real part of the) refractive index typically induces a split of the Mie resonances (leaky modes) involved, broadening the spectral region over which Mie-resonant absorption is enhanced for light incident over a broad angular range perpendicular and oblique to the NW axis. More importantly, it is shown that, for finite nanowires with dimensions of interest for light harvesting applications, the largest absorption cross sections (substantially larger than those predicted by Mie theory for infinite cylinders) are obtained for light incidence parallel to the NW axis, at which guided mode coupling (forbidden for infinite NWs) plays a crucial role in boosting absorption. This theoretical work provides a unified framework to tailor light absorption, with promising predictions for the design of broad-band and broad-angle solar light absorbers and photodetectors.

METHODS

Numerical Calculations. Finite-element-method-based numerical simulations were performed using commercial software COMSOL Multyphysics v4.3b. The simulated space consisted of a circular cylinder of length L and diameter D, representing the nanowire, and a cylinder of length $2L$ and radii $0.5L$ with its center coinciding with that of the nanowire. In the outer cylinder, an additional layer of thickness $0.2L$ was defined. The nanowire domain was set to be InP, with material constants taken from Palik's book,[39] while the rest of the space was set to be air ($n_{air} = 1$). The outer cylindrical layer was defined as a perfectly matched layer (PML) to absorb all the outgoing radiation. The meshing was done with the program built-in algorithm, which creates a tetrahedral mesh. The mesh maximum element size (MES), which limits the maximum size of the edges of the tetrahedrons, was set to be 10 nm in the domain representing the wire and 120 nm for the rest of the domains. The maximum element growth rate was set to 1.3 in the wire domain, and 1.35 in all remaining domains. Direct PARDISO solver was used to solve the problem. Simulations needed typically 30 GB of memory and took about 30 min per wavelength on a 32 CPUs computing station.

AUTHOR INFORMATION

Corresponding Author

*E-mail: j.sanchez@csic.es.

Notes

The authors declare no competing financial interest.

ACKNOWLEDGMENTS

We are grateful to J. Gómez Rivas and G. Grzela for fruitful discussions and suggestions. This work has been supported by the Spanish "Ministerio de Economía y Competitividad" (Projects Consolider-Ingenio EMET CSD2008-000666 and NANOPLAS+ FIS2012-31070).

REFERENCES

(1) Yan, R.; Gargas, D.; Yang, P. Nanowire photonics. *Nat. Photonics* **2009**, *3*, 569−576.
(2) Tian, B.; Kempa, T. J.; Lieber, C. M. Single nanowire photovoltaics. *Chem. Soc. Rev.* **2009**, *38*, 16−24.
(3) Wang, J.; Gudiksen, M. S.; Duan, X.; Cui, Y.; Lieber, C. M. Highly polarized photoluminescence and photodetection from single indium phosphide nanowires. *Science* **2001**, *293*, 1455−1457.
(4) Muskens, O. L.; Gómez Rivas, J.; Algra, R. E.; Bakkers, E. P. A. M.; Lagendijk, A. Design of light scattering in nanowire materials for photovoltaic applications. *Nano Lett.* **2008**, *8*, 2638−2642.
(5) Cao, L.; White, J. S.; Park, J.-S.; Schuller, J. A.; Clemens, B. M.; Brongersma, M. L. Engineering light absorption in semiconductor nanowire devices. *Nat. Mater.* **2009**, *8*, 643−7.
(6) Wu, P. M.; Anttu, N.; Xu, H. Q.; Samuelson, L.; Pistol, M.-E. Colorful InAs nanowire arrays: From strong to weak absorption with geometrical tuning. *Nano Lett.* **2012**, *12*, 1990−1995.
(7) Grzela, G.; Paniagua-Domínguez, R.; Barten, T.; Fontana, Y.; Sánchez-Gil, J. A.; Gómez Rivas, J. Nanowire antenna emission. *Nano Lett.* **2012**, *12*, 5481−5486.
(8) Huang, M. H.; Mao, S.; Feick, H.; Yan, H.; Wu, Y.; Kind, H.; Weber, E.; Russo, R.; Yang, P. Room-temperature ultraviolet nanowire nanolasers. *Science* **2001**, *292*, 1897−1899.
(9) Babinec, T. M.; Hausmann, B. J. M.; Khan, M.; Zhang, Y.; Maze, J. R.; Hemmer, P. R.; Loncar, M. A diamond nanowire single-photon source. *Nat. Nanotechnol.* **2010**, *5*, 195−199.
(10) Claudon, J.; Bleuse, J.; Malik, N. S.; Bazin, M.; Gregersen, N.; Sauvan, C.; Lalanne, P.; Gerard, J.-M. A highly efficient single-photon

DOI: 10.1021/acsphotonics.5b00112
ACS Photonics 2015, 2, 921−929

source based on a quantum dot in a photonic nanowire. *Nat. Photonics* **2010**, *4*, 174−177.
(11) Munsch, M.; Claudon, J.; Bleuse, J.; Malik, N.; Dupuy, E.; Gérard, J.-M.; Chen, Y.; Gregersen, N.; Mø rk, J. Linearly polarized, single-mode spontaneous emission in a photonic nanowire. *Phys. Rev. Lett.* **2012**, *108*, 077405.
(12) Kelzenberg, M. D.; Boettcher, S. W.; Petykiewicz, J. A.; Turner-Evans, D. B.; Putnam, M. C.; Warren, E. L.; Spurgeon, J. M.; Briggs, R. M.; Lewis, N. S.; Atwater, H. A. Enhanced absorption and carrier collection in Si wire arrays for photovoltaic applications. *Nat. Mater.* **2010**, *9*, 239−244.
(13) Brönstrup, G.; Jahr, N.; Leiterer, C.; Csáki, A.; Fritzsche, W.; Christiansen, S. Optical properties of individual silicon nanowires for photonic devices. *ACS Nano* **2010**, *4*, 7113−7122.
(14) Cao, L.; Fan, P.; Vasudev, A. P.; White, J. S.; Yu, Z.; Cai, W.; Schuller, J. A.; Fan, S.; Brongersma, M. L. Semiconductor nanowire optical antenna solar absorbers. *Nano Lett.* **2010**, *10*, 439−445.
(15) Garnett, E.; Yang, P. Light trapping in silicon nanowire solar cells. *Nano Lett.* **2010**, *10*, 1082−1087.
(16) Diedenhofen, S. L.; Janssen, O. T. A.; Grzela, G.; Bakkers, E. P. A. M.; Gómez Rivas, J. Strong geometrical dependence of the absorption of light in arrays of semiconductor nanowires. *ACS Nano* **2011**, *5*, 2316−2323.
(17) Wallentin, J.; Anttu, N.; Asoli, D.; Huffman, M.; Aberg, I.; Magnusson, M. H.; Siefer, G.; Fuss-Kailuweit, P.; Dimroth, F.; Witzigmann, B.; Xu, H. Q.; Samuelson, L.; Deppert, K.; Borgström, M. T. InP nanowire array solar cells achieving 13.8% efficiency by exceeding the ray optics limit. *Science* **2013**, *339*, 1057−1060.
(18) Diedenhofen, S. L.; Vecchi, G.; Algra, R. E.; Hartsuiker, A.; Muskens, O. L.; Immink, G.; Bakkers, E. P. A. M.; Vos, W. L.; Gómez Rivas, J. Broad-band and Omnidirectional Antireflection Coatings Based on Semiconductor Nanorods. *Adv. Mater.* **2009**, *21*, 973−978.
(19) Paniagua-Domínguez, R.; Abujetas, D. R.; Sánchez-Gil, J. A. Ultra low-loss, isotropic optical negative-index metamaterial based on hybrid metal-semiconductor nanowires. *Sci. Rep.* **2013**, *3*, 1507.
(20) Anttu, N. Geometrical optics, electrostatics, and nanophotonic resonances in absorbing nanowire arrays. *Opt. Lett.* **2013**, *38*, 730−732.
(21) Seo, K.; Wober, M.; Steinvurzel, P.; Schonbrun, E.; Dan, Y.; Ellenbogen, T.; Crozier, K. B. Multicolored vertical silicon nanowires. *Nano Lett.* **2011**, *11*, 1851−1856.
(22) Anttu, N.; Namazi, K. L.; Wu, P. M.; Yang, P.; Xu, H.; Xu, H. Q.; Håkanson, U. Drastically increased absorption in vertical semiconductor nanowire arrays: A non-absorbing dielectric shell makes the difference. *Nano Res.* **2012**, *5*, 863−874.
(23) Anttu, N.; Xu, H. Q. Efficient light management in vertical nanowire arrays for photovoltaics. *Opt. Express* **2013**, *21*, 27589−27605.
(24) Aghaeipour, M.; Anttu, N.; Nylund, G.; Samuelson, L.; Lehmann, S.; Pistol, M.-E. Tunable absorption resonances in the ultraviolet for InP nanowire arrays. *Opt. Express* **2014**, *22*, 29204−29212.
(25) Fountaine, K. T.; Kendall, C. G.; Atwater, H. A. Near-unity broadband absorption designs for semiconducting nanowire arrays via localized radial mode excitation. *Opt. Express* **2014**, *22*, A930−A940.
(26) Hu, L.; Chen, G. Analysis of optical absorption in silicon nanowire arrays for photovoltaic applications. *Nano Lett.* **2007**, *7*, 3249−3252.
(27) Wang, B.; Leu, P. W. Tunable and selective resonant absorption in vertical nanowires. *Opt. Lett.* **2012**, *37*, 3756−3758.
(28) Fountaine, K. T.; Whitney, W. S.; Atwater, H. A. Resonant absorption in semiconductor nanowires and nanowire arrays: Relating leaky waveguide modes to Bloch photonic crystal modes. *J. Appl. Phys.* **2014**, *116*, 153106.
(29) Stratton, J. A. *International Series in Pure and Applied Physics*; McGraw-Hill Book Company: New York, 1941.
(30) Arnbak, J. Leaky waves on a dielectric rod. *Electron. Lett.* **1969**, *5*, 41−42.
(31) Sammut, R.; Snyder, A. W. Leaky modes on circular optical waveguides. *Appl. Opt.* **1976**, *15*, 477−482.
(32) Bohren, C. F.; Huffman, D. R. *Absorption and Scattering of Light by Small Particles*; Wiley: N.Y., 1998.
(33) Ruda, H.; Shik, A. Polarization-sensitive optical phenomena in semiconducting and metallic nanowires. *Phys. Rev. B* **2005**, *72*, 1−11.
(34) Ruda, H. E.; Shik, A. Polarization-sensitive optical phenomena in thick semiconducting nanowires. *J. Appl. Phys.* **2006**, *100*, 024314.
(35) Zhan, Y.; Zhao, J.; Zhou, C.; Alemayehu, M.; Li, Y.; Li, Y. Enhanced photon absorption of single nanowire α-Si solar cells modulated by silver core. *Opt. Express* **2012**, *20*, 11506−11516.
(36) Mann, S. A.; Garnett, E. C. Extreme light absorption in thin semiconductor films wrapped around metal nanowires. *Nano Lett.* **2013**, *13*, 3173−3178.
(37) Grzela, G.; Paniagua-Domínguez, R.; Barten, T.; van Dam, D.; Sánchez-Gil, J. A.; Rivas, J. G. Nanowire antenna absorption probed with time-reversed fourier microscopy. *Nano Lett.* **2014**, *14*, 3227−3234.
(38) Hu, J.; Menyuk, C. R. Understanding leaky modes: slab waveguide revisited. *Adv. Opt. Photonics* **2009**, *1*, 58−106.
(39) Palik, E. D. *Handbook of Optical Constants of Solids*; Academic Press: New York, 1998; Vol. *1*; p 900.
(40) Rybin, M. V.; Samusev, K. B.; Sinev, I. S.; Semouchkin, G.; Semouchkina, E.; Kivshar, Y. S.; Limonov, M. V. Mie scattering as a cascade of Fano resonances. *Opt. Express* **2013**, *21*, 825−828.
(41) Paniagua-Domínguez, R.; Grzela, G.; Gómez Rivas, J.; Sánchez-Gil, J. A. Enhanced and directional emission of semiconductor nanowires tailored through leaky/guided modes. *Nanoscale* **2013**, *5*, 10582−10590.

DOI: 10.1021/acsphotonics.5b00112
ACS Photonics 2015, 2, 921−929